Stability Analysis for DC-Link Voltage Controller Design in Single-Stage Single-Phase Grid-Connected PV Inverters

Faicel EL Aamri, Hattab Maker, Dezso Sera, *Senior Member, IEEE*, Sergiu Spataru, Josep M. Guerrero, *Fellow, IEEE*, Abderrahim Fakkar, and Azeddine Mouhsen

***Abstract*—The dc-link voltage control is vitally important to ensure the operation of photovoltaic (PV) system at the maximum power voltage, where its performance affects the power quality injected into the grid. In this work, we propose a method, based on the Lyapunov function, for investigating the control system stability, during the design of a nonlinear dc-link voltage controller for single-stage single-phase grid-connected PV inverters. Furthermore, we demonstrate analytically that the non-linearity of the PV string's power-voltage (P-V) curve leads to system instability. Consequently, this article proposes an adaptive dc-link voltage controller, built from the P-V curve, as an application in order to establish a stability criterion. Simulations and experimental validations have been carried out on a grid-connected single-stage single-phase PV inverter test platform. The results confirm the feasibility of the analytical study developed in this article, as well as the proposed dc-link voltage controller with and without the stability analysis.**

***Index Terms*—Lyapunov stability, maximum power point tracking (MPPT), perturb and observe (P&O), single-stage single-phase PV inverters.**

I. Introduction

THE penetration of solar energy in the electricity network has been rapidly increasing worldwide [1]. Hence, grid-connected photovoltaic (PV) inverters have received significant attention in research [2], [3], considering the impact of wide-scale distributed PV generation on the grid stability [4]. From a hardware topology point-of-view, single-stage PV inverters are widespread due to their simpler structure (only one conversion is required) [5], [6], [7], which results in lower cost and higher efficiency [8]. These topologies are popular, especially in central inverters [9]. However, in these topologies, the inverter as shown in Fig. 1 must provide all the functions required by a grid-connected PV application, including maximum power point tracking (MPPT), meaning the dc-link voltage cannot be maintained constant [10].

For instance, as shown in Fig. 2, the main components necessary to control this topology are as follows.

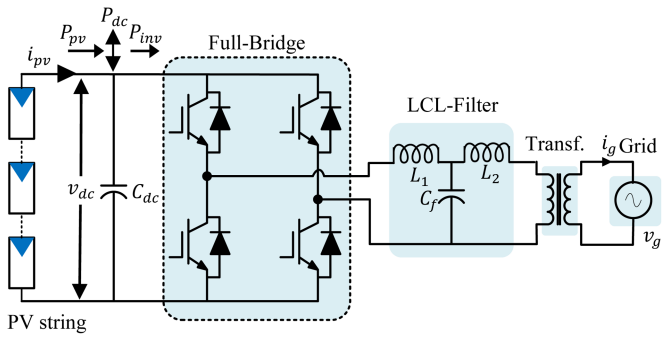

Fig. 1. System configuration of single-stage single-phase grid-connected PV inverter.

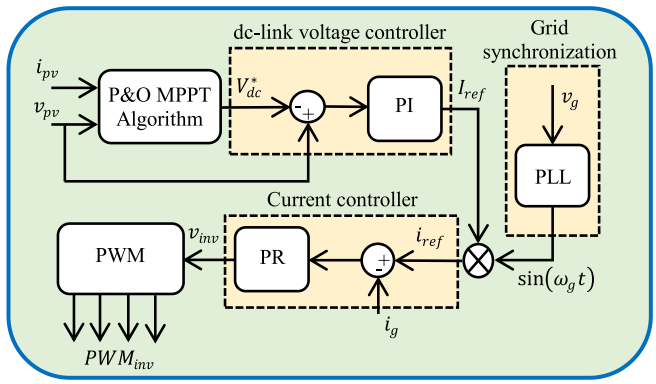

Fig. 2. Control structure for single-stage single-phase grid-connected PV inverter (PI—Proportional Integral, PLL—Phase Locked Loop, PR—Proportional Resonant, PWM—Pulsewidth Modulation. Note that, being a single stage inverter, the PV string voltage v_{pv} is equal to dc-link voltage v_{dc}).

Manuscript received 28 October 2022; revised 2 January 2023, 20 February 2023, 22 March 2023, and 27 March 2023; accepted 27 March 2023. Date of publication 12 April 2023; date of current version 15 July 2023. *(Corresponding author: Faicel EL Aamri.)*

Faicel EL Aamri and Abderrahim Fakkar are with the Laboratory of Materials, Energy and Control Systems, Faculté des Sciences et Techniques, Hassan II University of Casablanca, 28806 Mohammedia, Morocco (e-mail: f.elaamri@gmail.com; fakkara@yahoo.fr).

Hattab Maker is with the University Hassan 1, LISA, ESTB, 26000 Settat, Morocco (e-mail: hattabmaker@gmail.com).

Dezso Sera is with the Faculty of Science and Engineering, Queensland University of Technology, Brisbane, QLD 4000, Australia (e-mail: dezso.sera@qut.edu.au).

Sergiu Spataru and Josep M. Guerrero are with the Department of Energy Technology, Aalborg University, DK-9220 Aalborg, Denmark (e-mail: ssp@et.aau.dk; joz@et.aau.dk).

Azeddine Mouhsen is with the University Hassan 1, LRMI, FSTS, 26000 Settat, Morocco (e-mail: az.mouhsen@gmail.com).

Color versions of one or more figures in this article are available at https://doi.org/10.1109/JPHOTOV.2023.3263253.

Digital Object Identifier 10.1109/JPHOTOV.2023.3263253

1) MPPT algorithm, mandatory to maximize the power yield from the PV string.
2) Current controller [11], [12], [13].
3) DC-link voltage controller.
4) Grid synchronization function used to track the fundamental component of the grid voltage [14].

The MPPT algorithm and the dc-link voltage controller are denoted together as an outer-loop, which provides the magnitude of the reference grid current I_{ref}. Then, the inner-loop is designed to control the grid current i_g [15]. It is well known that the PV power-voltage (P-V) characteristic is nonlinear and varying with the ambient conditions (solar irradiance and temperature). Hence, to track the maximum power on this characteristic, the first subsystem in the outer-loop (MPPT, e.g., P&O) provides a reference voltage V_{dc}^* during its periodical operation. Next, the voltage controller, which is based on a proportional-integral (PI) controller, in the conventional structure, determines the magnitude of the reference grid current, to control the PV string working at the reference voltage V_{dc}^*.

Designing an efficient dc-link voltage controller is vitally important, in order to guarantee the reliable operation of the power flow. As mentioned before, the most frequently used dc-link voltage controller is the PI controller, where its parameters (K_P- proportional gain and K_I- integral gain) are tuned for the rated power in the standard test conditions (STC) to achieve a set of requirements, such as global stability, which is the focus of this article, and good transient performances.

In the literature, several approaches have been proposed for grid-tied PV systems. For instance, a self-tuned PI controller with an anti-windup function has been proposed in [16]. In [17], and [18] an improved PI controller with a nonlinear disturbance observer is proposed for a hybrid ac/dc microgrid. In the same way, various linear methods have been proposed in [19], [20], [21], and [22] to reduce the required dc-link capacitor with an improved dynamic performance of the dc-link voltage control.

In [23], the authors propose a nonlinear control based on the Lyapunov function, where it requires having a dc-link capacitor sufficiently large. Alternatively, in [24], the authors have applied a modification on the same approach on the three-phase PV inverter that requires a smaller dc-link capacitor, as the power on the dc side has no oscillations [25]. Additional work in [26] proposes an energy-balance control strategy that is applied to a cascaded H-bridge multilevel inverter. In addition, a hybrid control technique was proposed in [27], where the control scheme comprises a current control loop based on passivity theory.

Furthermore, for a two-stage topology, a H_∞ method has been designed in [28] for a weak grid operation. However, the nonlinearity of the PV string's P-V curve has been ignored. The same feature was ignored in [29], where the authors proposed a nonlinear PI predictive controller. Another approach that takes into account the nonlinearity has been proposed in [30], which eliminates the voltage-loop control.

To sum up, it can be observed from the references, that the dc-link voltage-loop control has received remarkable interest. Even so, an important characteristic of these systems, which appears to have received no attention in the literature is that the error signal $\varepsilon_{dc} = (V_{ref} - V_{dc})$ at the input of the dc-link voltage controller is reversed (see Fig. 2) when compared to the classical control-loop. Otherwise, the system will be stuck at the open circuit voltage of PV string at startup. Then, will no longer pursue the maximum power point (MPP).

In this regard, the contribution of this article is to propose a stability analysis for single-phase grid-connected PV inverters, to deal with the stability criterion of the PV system when developing a new nonlinear dc-link voltage controller. Also, this article proposes an adaptive dc-link voltage controller, built from the P-V curve, as an application in order to establish a stability criterion. While the dc-link capacitor has a direct influence on the energy transfer from dc side (PV string) to ac side (grid) as the decoupling storage element [31], [32], the converters output (grid side) filter normally has a much lower amount of stored energy. Therefore, its effect on the energy transmission can be neglected [33]. Hence, for the stability study, the Lyapunov function is formed based only on the variation of stored energy in the dc-link capacitor.

The remainder of this article is organized as follows: in Section II, a stability study related to the effect of the nonlinear P-V curve in terms of the dc-link voltage will be presented, in addition to an adaptive dc-link voltage controller based on the P-V curve. Section III aims to validate the analytical demonstration through simulations. In Section IV, the operation of the proposed controller with and without a stability analysis is verified through experimental tests. Finally, Section V concludes the article.

II. Stability Analysis

In this section, we analyze the effect of the nonlinearity of the PV string's P-V curve on the dc-link voltage behavior, considering two cases:

1) without using a voltage-loop controller, and
2) using a voltage-loop controller.

A. Power Flow Description

As presented in Fig. 1, the grid-connected PV inverter is modeled based on the power flow, where the power balance can be written as the equation below:

$$p_{pv}\left(v_{dc}\right) = p_{dc} + p_{inv} \tag{1}$$

where $p_{pv}(v_{dc})$ is the instantaneous power from the PV string, p_{inv} is the instantaneous power drawn by the inverter, and p_{dc} is the instantaneous power across the dc-link capacitor expressed by the following equation:

$$p_{dc} = C_{dc} v_{dc} \frac{dv_{dc}}{dt} \tag{2}$$

where v_{dc} is the measured dc-link voltage and C_{dc} is the dc-link capacitance. Assuming no power losses in the PV inverter, $p_{inv} = p_{grid}$, the latter term denoting the instantaneous power fed into the grid and expressed as

$$p_{grid} = P_{grid} - P_{grid} \cos\left(2\omega_g t\right) \tag{3}$$

where $P_{grid} = V_g\, I_g$, V_g is the RMS of the grid voltage, I_g is the RMS of the injected grid current, and ω_g is the grid pulsation.

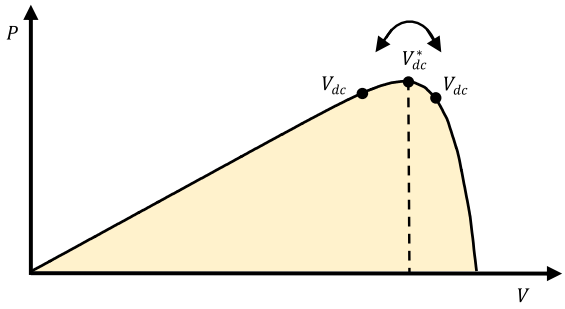

Fig. 3. PV string characteristic, showing the dc-link voltage oscillates on either side of the MPP.

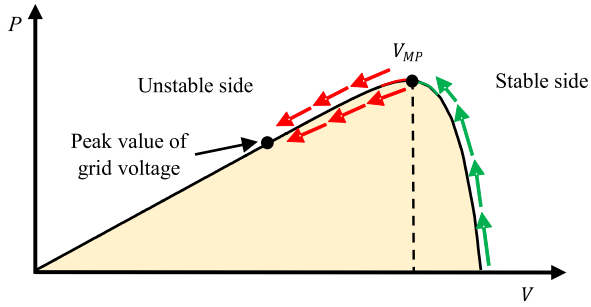

Fig. 4. Stability criterion in the different part of the P-V characteristic, where V_{MP} is the voltage at the maximum power.

In practice, the measured dc-link voltage consists of two components, an average value added to a ripple with a small amplitude and double the grid frequency. A notch filter in the dc-link voltage control-loop can mitigate the effect of this ripple [34]. Accordingly, we assume that V_{dc} has no ripple component in the following equations. In addition, we assume that the pulsating grid power $P_{grid}\cos(2\omega_g t)$ is mitigated as well.

From (1) and (2), we derive the following equation:

$$P_{pv}\left(V_{dc}\right) = P_{grid} + C_{dc}V_{dc}\frac{dV_{dc}}{dt}. \tag{4}$$

Furthermore, it should be mentioned that to regulate the power fed into the grid involves that P_{grid} is equal to P_{ref}, where P_{ref} denotes the reference power (the amount of power that will be injected in the grid). From (4), we develop (5) for controlling the output power of the inverter as

$$P_{ref} = P_{pv} - C_{dc}V_{dc}\frac{dV_{dc}}{dt} \tag{5}$$

where P_{pv} is the power feedforward component of the control law.

B. Lyapunov Function

Lyapunov stability theory is typically used in the analysis of nonlinear systems. A Lyapunov function $V(x)$ is a scalar energy that permits to define the system states. Hence, in this article, it will be formed based on the variation of stored energy in the dc-link capacitor, assuming that other components such as the LCL filter have no effect on the system stability [33]. Then, the Lyapunov function candidate can be written as

$$V(E) = \frac{C_{dc}^2}{4}\left(V_{dc}^{*2} - V_{dc}^2\right)^2 \tag{6}$$

where $V(E)$ is taken as a positive function, E refers to the stored energy across the dc-link capacitor, V_{dc}^* is the reference voltage given by the MPPT algorithm, which is assumed equal to the MPP voltage of the PV string, V_{MP}, shown in Fig. 4, V_{dc} is the actual measured dc-link voltage as well and it can be on either side of the P-V curve, as shown in Fig. 3.

On the other hand, according to [35], a system is globally stable if $V(E)$ achieves the succeeding conditions as

$$V(0) = 0 \tag{7}$$

$$V(E) > 0 \text{ for all } V(E) \neq 0 \tag{8}$$

$$V(E) \to \infty \text{ as } |E| \to \infty \tag{9}$$

$$\frac{dV(E)}{dt} < 0 \text{ for all } E \neq 0. \tag{10}$$

It can be noted that the fourth condition implies that the system is globally stable if the full stored energy is continuously dissipated $(V(E) \times (dV(E)/dt) < 0)$, meaning that the system is permanently sliding to an equilibrium point.

Hence, the chosen Lyapunov function satisfies the aforementioned properties [conditions 1, 2, and 3 in (7), (8), and (9)] and its derivative $dV(E)/dt$ is given by (11) as

$$\frac{dV(E)}{dt} = \frac{C_{dc}^2}{2}\left(V_{dc}^{*2} - V_{dc}^2\right)\left(0 - 2V_{dc}\frac{dV_{dc}}{dt}\right) \tag{11}$$

from which the expression (11) is obtained in the form

$$\frac{dV(E)}{dt} = -C_{dc}^2 V_{dc}\frac{dV_{dc}}{dt}\left(V_{dc}^{*2} - V_{dc}^2\right). \tag{12}$$

Moreover, separating the last term in (12), yields

$$\frac{dV(E)}{dt} = -C_{dc}^2 V_{dc}\frac{dV_{dc}}{dt}\left(V_{dc}^* - V_{dc}\right)\left(V_{dc}^* + V_{dc}\right). \tag{13}$$

Substituting (5) into (13) gives

$$\frac{dV(E)}{dt} = C_{dc}\left(P_{ref} - P_{pv}\right)\left(V_{dc}^* - V_{dc}\right)\left(V_{dc}^* + V_{dc}\right). \tag{14}$$

In fact, based on (14), the sign of the derivative of Lyapunov function can be determined. Obviously, it depends on the power variation in terms of the voltage difference. As mentioned previously, we considered two cases to evaluate the system stability convergence.

1) Case 1–Without Using a Voltage Controller: Based on (14), this case aims to show how the nonlinearity of the P-V curve of the PV string can cause the instability of the PV system. The last term $(V_{dc}^* + V_{dc})$ in (14) is positive. Then, we assume in both cases that the term $(P_{ref} - P_{pv})$ is always positive (based on MPPT algorithm, e.g., P&O as long as the operating point does not oscillate around MPP, otherwise, it will either be positive or negative), regardless of the operating point position; on the right side or the left side of the P-V curve, as presented in Fig. 3.

Once the operating point is located on the right side of MPP, as shown in Fig. 3, it will result in $V_{dc}^* - V_{dc} < 0$. Therefore, it sets the derivative of Lyapunov function to negative, which means based on Lyapunov theory [condition 4 in (10)] that the

system remains stable on that side. Hence

$$if \quad V_{dc} > V_{dc}^* \Rightarrow \frac{dV(E)}{dt} < 0. \tag{15}$$

Similarly, if the operating point is located on the left side of MPP as shown in Fig. 3, results in $(V_{dc}^* - V_{dc})$ being positive. It sets the derivative of Lyapunov function to positive and the system turns into an unstable state on that side. Hence

$$if \quad V_{dc} < V_{dc}^* \Rightarrow \frac{dV(E)}{dt} > 0. \tag{16}$$

Ultimately, based on the achieved results, the nonlinearity of the PV string's P-V curve is significantly affecting the system stability. For instance, if the operating point is located on the right side, the system is stable, which means that the operating point moves toward the MPP, as shown in Fig. 4. Once the operating point is moved to the left side, based on the expression (16), the system turns into an unstable state. Accordingly, the operating point trajectory moves towards a local equilibrium point, which is the peak of grid voltage as shown in Fig. 4. Hence, the voltage balance is achieved and the power flow is interrupted.

2) Case 2–Using a Voltage Controller: Contrary to the first case, this case aims to ensure a global stability, in which a voltage-loop controller is employed to regulate directly the energy across the dc-link capacitor. Therefore, the (17) can be written as

$$C_{dc} V_{dc} \frac{dV_{dc}}{dt} = K\left(V_{dc}^* - V_{dc}\right) \tag{17}$$

where K is a positive gain and denotes the voltage PI controller, neglecting the integral effect [36]. The expression $(V_{dc}^* - V_{dc})$ in the equation above refers to the conventional error signal at the input of the controller. Substituting (17) into (13) gives

$$\frac{dV(E)}{dt} = -C_{dc} K (V_{dc}^* - V_{dc})^2 \left(V_{dc}^* + V_{dc}\right) \tag{18}$$

leading to a permanent negative equation. Since $(V_{dc}^* - V_{dc})^2$ is positive and K is positive as well, which means achievement of global stability, regardless of the location of the operating point on the nonlinear P-V curve, rather than a local stability point as was typically in the first case.

Next, substituting (17) into the equation that controls the output power (5) yields

$$P_{ref} = P_{pv} - K\left(V_{dc}^* - V_{dc}\right). \tag{19}$$

In fact, the controlled variable is the injected grid current, since it is assumed that the grid voltage is fixed. Therefore, (19) can be rewritten as

$$I_{ref} = 2\frac{P_{pv} - K\left(V_{dc}^* - V_{dc}\right)}{\hat{V}_g} \tag{20}$$

where $\hat{V}_g$ is the peak value of grid voltage. Equation (20) shows the origin of the reverse error signal $\varepsilon_{dc} = (V_{dc}^* - V_{dc})$ at the input of the PI controller, where it is demonstrated based on the Lyapunov stability theorem

$$I_{ref} = 2\frac{P_{pv} + K\left(-V_{dc}^* + V_{dc}\right)}{\hat{V}_g}. \tag{21}$$

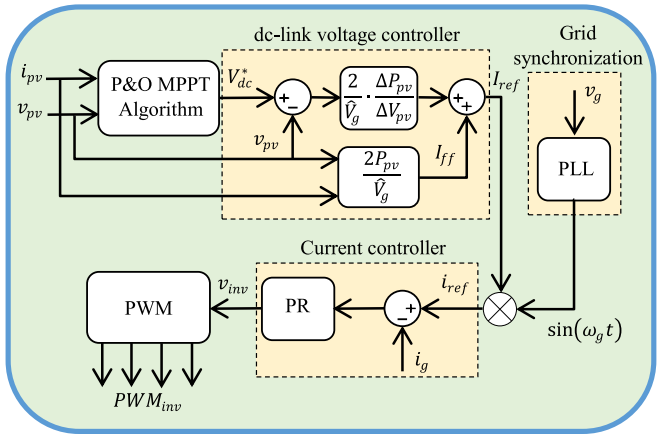

Fig. 5. General control structure of single-stage PV inverter using the proposed dc-link voltage controller, where V_{pv} and P_{pv} are the average values of the PV string's voltage and power, respectively. v_g, i_g, and ω_g are the instantaneous grid voltage, grid current, and grid frequency, respectively. $\hat{V}_g$ is the peak value of grid voltage and given by PLL.

Compared to the control structure presented in Fig. 2, (21) includes the power feedforward P_{pv}, that enhances the MPPT dynamics, it is added to the PI controller output and it is not shown in Fig. 2. Indeed, both structures (with or without power feed forward as shown in Fig. 5) are equivalent and the proof remains valid for both structures.

C. Proposed Adaptive DC-Link Voltage Controller

The idea behind the adaptive dc-link voltage controller consists in linearizing the P-V curve step by step. Accordingly, this process requires three points. Notice that the MPPT algorithm (e.g., P&O) provides a reference voltage during its periodical operation, where the PV output power is measured and compared with the previous power. Then, the reference voltage is increased or decreased to check whether the power is increased or decreased. Consequently, we obtain three points on the P-V curve, P_{k-1} the previous measured power, P_k the available PV power and P_{k+1} is the predicted PV power which corresponds to the new voltage reference. As a minor perturbation is introduced to cause the power variation of the PV string, then it can be stated that the slope bounded through these three points on the P-V curve is linear. Hence, we get

$$\frac{P_{k+1} - P_k}{V_{k+1} - V_k} = \frac{P_k - P_{k-1}}{V_k - V_{k-1}} \tag{22}$$

where V_{k-1} is the previous measured voltage, V_k is the new measured PV voltage, and V_{k+1} is the reference voltage. Therefore, the predicted power can be calculated as

$$P_{k+1} = P_k + \frac{dP_{pv}}{dV_{pv}}\left(V_{k+1} - V_k\right) \tag{23}$$

where $dP_{pv} = P_k - P_{k-1}$ and $dV_{pv} = V_k - V_{k-1}$. In fact, the predicted power denotes the reference power and can be reformulated as

$$P_{ref} = P_{pv} + \frac{dP_{pv}}{dV_{pv}}\left(V_{dc}^* - V_{dc}\right) \tag{24}$$

TABLE I
PARAMETERS FOR SIMULATION AND EXPERIMENT

PV power	1 kW
V_{MP}	455 V
I_{sc}	2.42 A
V_{oc}	568 V
dc-link capacitor	1200 μF
Switching frequency	8000 Hz
PI controller parameters	$K_p = 8 \times 10^{-5}$, $K_I = 8{,}5 \times 10^{-4}$
PR controller parameters	$K_p = 10$, $K_r = 1000$
LCL-filter	$L_1 = 2.6$ mH, $C_f = 2.2$ μF $L_2 = 0.41$ mH
Grid nominal voltage (RMS)	230 V
Grid nominal frequency	50 *Hz*

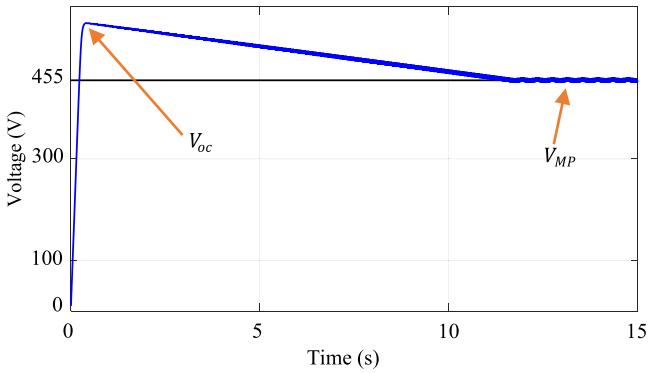

Fig. 6. Start waveform for dc-link voltage.

where $V_{dc}^* = V_{k+1}$, $V_{dc} = V_k$ and $P_{pv} = P_k$. Thus, Fig. 5 presents the adaptive dc-link voltage controller based on (25) as

$$I_{ref} = I_{ff} + \frac{2}{\hat{V}_g} \frac{\Delta P_{pv}}{\Delta V_{pv}} \varepsilon_{dc} \tag{25}$$

where I_{ff} denotes the current feedforward and is equal to $2P_{pv}/\hat{V}_g$, ΔP_{pv} represents the variation of the PV power, and ΔV_{pv} represents the variation of the dc -link voltage. Note that $V_{pv} = V_{dc}$ as shown in Fig. 5.

III. SIMULATION STUDY

This section evaluates the theoretical stability based on Lyapunov function using simulations through MATLAB/Simulink. In this regard, the control strategy used is shown in Fig. 2 for a single-phase grid-connected PV inverter. The parameters of PV system used in the simulation and experimental tests are summarized in Table I. To note that the parameters selected for P&O are: $f_{MPPT} =$ 10 Hz – tracking frequency, and $\Delta V_{MPPT} = 1V$ - increment step voltage, so that to reduce the oscillations around the MPP and therefore the losses in steady-state [37].

Fig. 6 shows the start waveform for the dc-link voltage, where it is shown that the MPPT algorithm starts to follow the MPP from the right side once the dc-link capacitor is fully charged, its value is equal to open circuit voltage V_{oc} of the PV string. Then, the dc-link voltage capacitor oscillates around the MPP in steady-state.

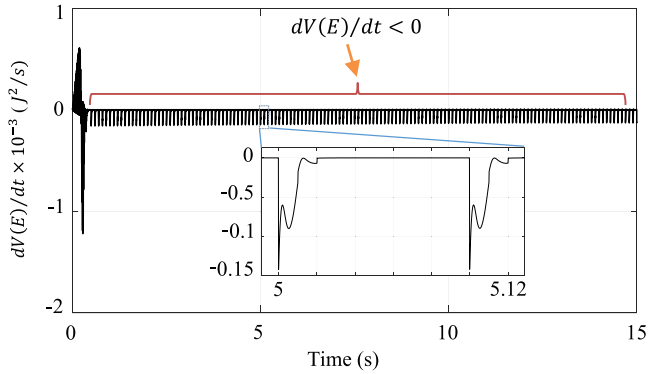

Fig. 7. Derivative of the Lyapunov function.

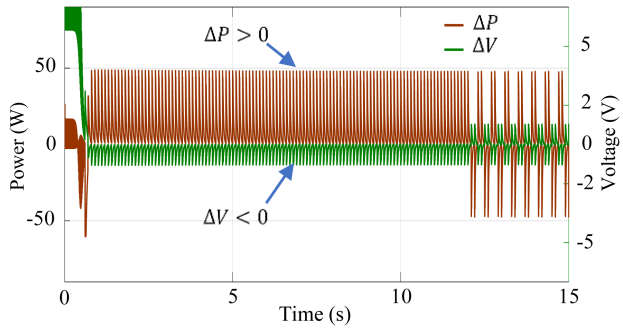

Fig. 8. Simulation results showing ΔP and ΔV waveforms based on (14).

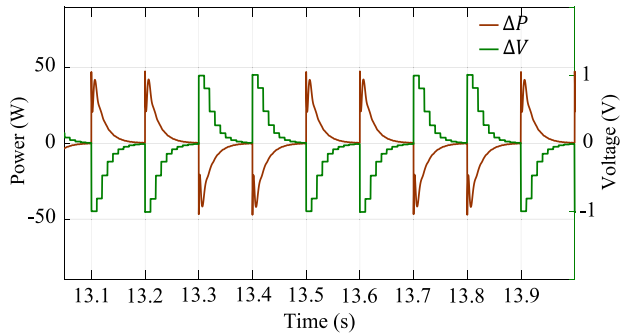

Fig. 9. Simulation results of ΔP and ΔV waveforms in the vicinity of MPP.

Therefore, Fig. 7 shows the derivative of the Lyapunov function based on (14), where it can be observed that $dV(E)/dt$ is permanently negative. Furthermore, it can be seen that at each generation of the reference current, the derivative of Lyapunov function decreases. Thereafter, it converges towards zero in the steady-state, which keeps the system stable.

Also, Fig. 8 shows the waveforms of $\Delta P = (P_{ref} - P_{pv})$ and $\Delta V = (V_{dc}^* - V_{dc})$ in the trajectory to follow the MPP from the right side to the MPP voltage of the PV string, in steady-state. Where P_{ref} is generated by the dc-link voltage controller and V_{dc}^* is given by MPPT algorithm (e.g., P&O). Hence, Fig. 9 shows the waveforms of ΔP and ΔV around MPP, where it is evident that the two terms have opposite signs. This means if ΔV is positive, ΔP should be negative and vice versa, necessary to keep the derivative of Lyapunov function

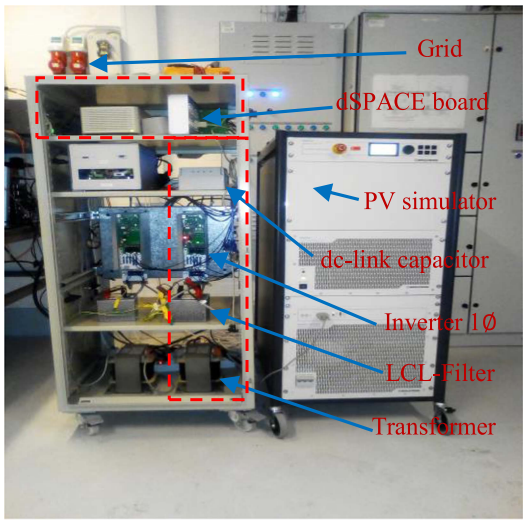

Fig. 10. Photograph of the single-phase single-stage grid-connected PV inverter setup used in this work.

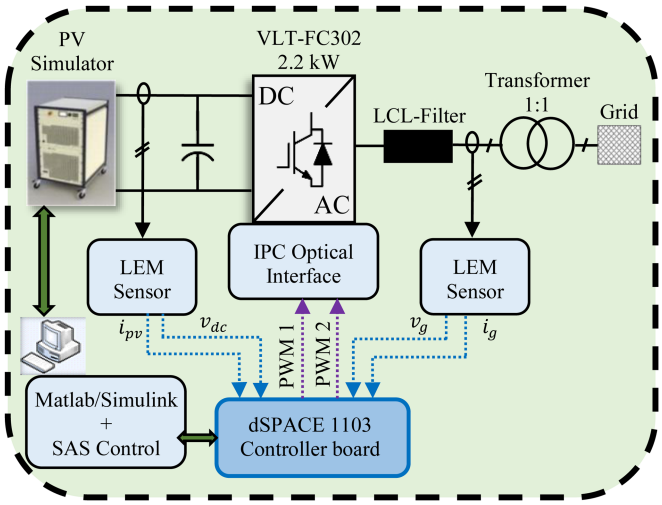

Fig. 11. Layout of the experimental setup.

continuously negative and consequently to ensure the system stability.

IV. Experimental Results

This section presents an application of the above results on an experimental setup, shown in Fig. 10, that consists of a PV simulator (Regatron TopCon Quadro with a linear post-processing unit TC.LIN) to emulate a preloaded I-V curve of the PV string, a dSPACE 1103 controller board, a 2.2kW Danfoss VLT-FC302 inverter, grid-connected through an LCL filter and a single-phase transformer for the galvanic isolation, the system parameters were listed in Table I. Furthermore, as shown in Fig. 11, four suitable LEM sensors are connected to dSPACE 1103 controller board and are used to measure the dc-link voltage, the PV string current, the grid voltage, and the grid current. The measured data are viewed in real time in ControlDesk software and then stored in MATLAB environment.

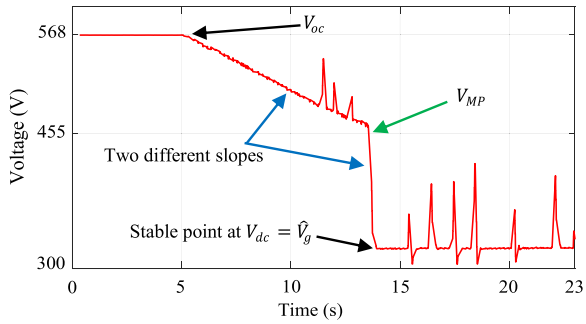

Fig. 12. Experimental start waveform of dc-link voltage (using the proposed controller as shown in Fig. 5), showing the tracking of MPP. Once the dc-link voltage reaches the MPP, the system turns into unstable state, then the operating point moves to a stable state.

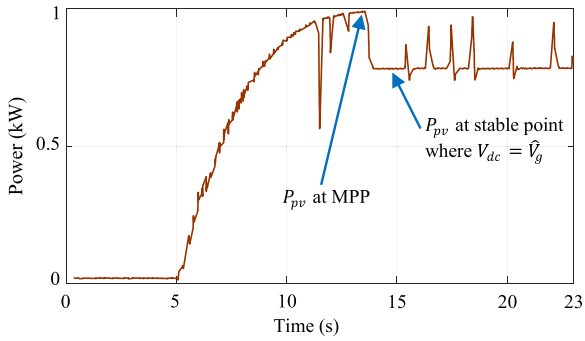

Fig. 13. Experimental start waveform of PV power (using the proposed controller), showing the tracking of MPP. Once PV power reach the MPP, the system turns into unstable state, then the operating point moves to a stable state.

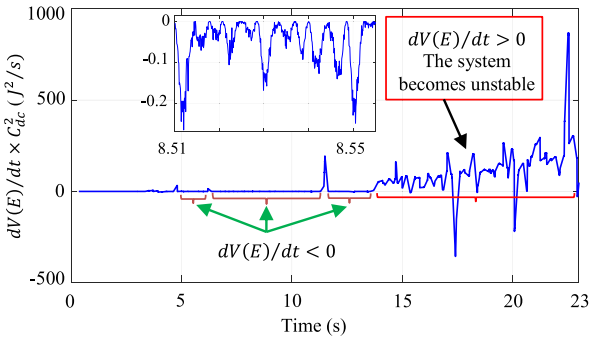

Fig. 14. Experimental result of the derivative of Lyapunov function (using the proposed controller as shown in Fig. 5). In order to help visualising the full range on the graph, it has been multiplied by C_{dc}^2.

For the experimental procedure, to examine the stability of the proposed controller, shown in Fig. 5, the startup case will be considered, where the operating point is located on the right side of MPP and the dc-link voltage is equal to open circuit voltage of PV string. Note that the gain multiplied by the error ε_{dc} on (25) depends on the P-V curve of the PV string and is determined with frequency $f_{MPPT} = 10$ Hz.

Figs. 12 and 13 show the dc-link voltage response and PV power. Besides, Fig. 14 shows the experimental results of the derivative of Lyapunov function based on (14), where it can be seen from the results, that during the tracking process of MPP, the derivative of Lyapunov function remains negative. Once the

dc-link voltage is getting closer to MPP, it turns into positive, which means that the system is moved to an unstable state, the operating point drops into the left side as well, down to the peak value of grid voltage $\hat{V}_g$.

Furthermore, it can be seen from Figs. 12 and 13 that the proposed controller attempts to track the MPP from the left side of MPP. However, the Lyapunov function remains positive, as shown in Fig. 14.

In order to take into consideration the stability analysis developed in (14) and validated by simulation, the proposed controller shown in (25) is based on (24). Thus, if the operating point is located on the right side of MPP, it can be stated that $dP_{pv}/dV_{pv} < 0$ and $V_{dc}^* - V_{dc} < 0$. Consequently, from the outcome of (24) we get

$$\left.\begin{array}{l} P_{ref} > P_{pv} \\ \Delta P > 0 \\ \Delta V < 0 \end{array}\right\} \Rightarrow \frac{dV(E)}{dt} < 0. \tag{26}$$

As a result of (14), since the derivative of Lyapunov function is negative, the system remains stable. In the other case, if the operating point is moved to the left side of MPP yields $dP_{pv}/dV_{pv} > 0$ and $V_{dc}^* - V_{dc} > 0$. Hence

$$\left.\begin{array}{l} P_{ref} > P_{pv} \\ \Delta P > 0 \\ \Delta V > 0 \end{array}\right\} \Rightarrow \frac{dV(E)}{dt} > 0 \tag{27}$$

which means that the system turns into an unstable state.

To achieve global stability, we focus first on the PI dc-link voltage controller as written in (19), to find out how it behaves with respect to the nonlinearity of the PV string's P-V curve. Hence, according to (17), if the operating point is located on the right side of MPP yields

$$\begin{cases} p_{dc} = C_{dc} V_{dc} \frac{dV_{dc}}{dt} = K\left(V_{dc}^* - V_{dc}\right) \\ K\left(V_{dc}^* - V_{dc}\right) < 0 \end{cases} \Rightarrow \frac{dp_{dc}}{dt} < 0. \tag{28}$$

Next, the outcome of (28) can be used in (19) as follows:

$$\begin{cases} P_{ref} = P_{pv} - K\left(V_{dc}^* - V_{dc}\right) \\ -K\left(V_{dc}^* - V_{dc}\right) > 0 \end{cases} \Rightarrow P_{ref} > P_{pv}. \tag{29}$$

Based on the above equations, it can be concluded that the PI controller injects the power into the grid by returning the stored energy in the dc-link capacitor (that comes from PV string) to the grid simultaneously. Similarly, if the operating point is located on the left side of MPP yields

$$\begin{cases} p_{dc} = C_{dc} V_{dc} \frac{dV_{dc}}{dt} = K\left(V_{dc}^* - V_{dc}\right) \\ K\left(V_{dc}^* - V_{dc}\right) > 0 \end{cases} \Rightarrow \frac{dp_{dc}}{dt} > 0 \tag{30}$$

$$-K\left(V_{dc}^* - V_{dc}\right) < 0 \Rightarrow P_{ref} < P_{pv} \tag{31}$$

which means that the PI controller in (30) stores the energy in the dc-link capacitor. At the same time in (31), the PI controller controls the grid to take less than the available power ($P_{ref} < P_{pv}$) from the PV string on the left side of MPP, based on Fig. 3. Therefore, after the above results shown in (29) and (31), it is possible to add to the equation of the adaptive controller a parameter that takes two values, in order to achieve global stability as in the following equation:

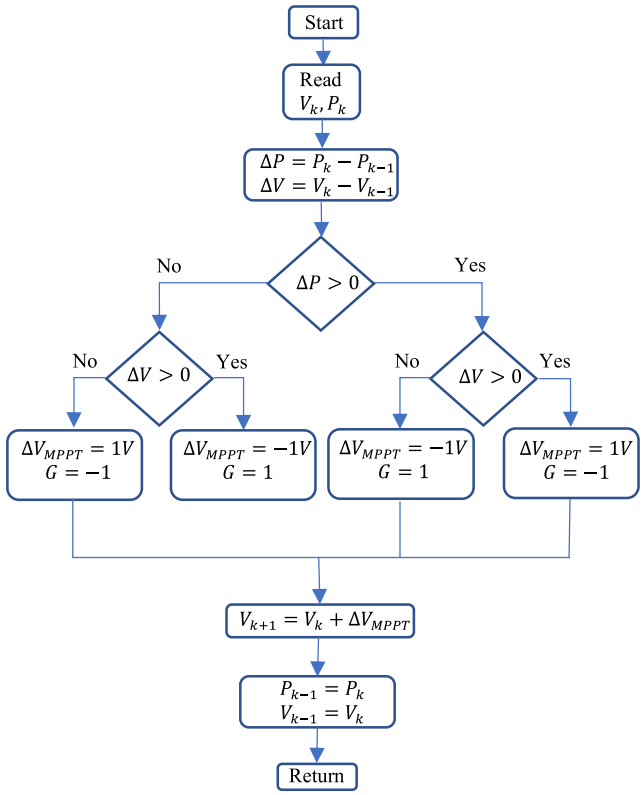

Fig. 15. Flowchart of the P&O algorithm, taking into account the parameter for the system stability.

$$P_{ref} = P_{pv} + G\frac{dP_{pv}}{dV_{pv}}\left(V_{dc}^* - V_{dc}\right) \tag{32}$$

where G can be $\{-1\ or\ 1\}$ as shown in Fig. 15. G is equal to 1 if the operating point is located on the right side of MPP. Then, the system remains stable by default. On the other side, G is equal to -1 if the operating point is located on the left side of MPP, so that the derivative of the Lyapunov function shown on (14) remains negative.

Hence, the proposed adaptive dc-link voltage controller turns into the following equation:

$$I_{ref} = I_{ff} + G\frac{2}{\hat{V}_g}\frac{\Delta P_{pv}}{\Delta V_{pv}}\varepsilon_{dc}. \tag{33}$$

Therefore, it will be considered two cases to examine whether the system converges from an operating point on either side of the MPP. The first one is from the right side of MPP, where the dc-link capacitor is fully charged and its voltage is equal to the open circuit voltage of PV string.

Figs. 16 and 17 show the PV voltage tracking response and the PV power. Moreover, Fig. 18 shows the derivative of Lyapunov function, where it can be seen that it remains negative even if the operating point oscillates around the MPP, which means achievement of the global stability.

Similarly, the second experimental case is carried out from the left side of MPP, particularly from the stable point where the dc-link voltage is equal to the peak grid voltage, in which the

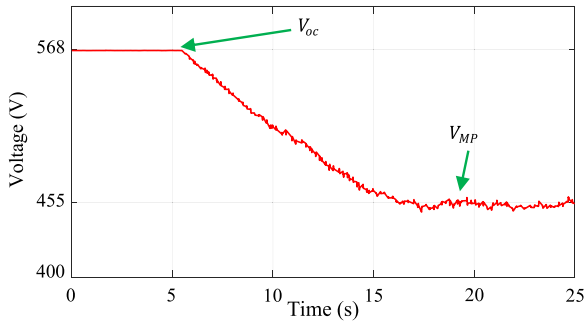

Fig. 16. Experimental responses of PV voltage from the right side of MPP, using the proposed controller based on (33).

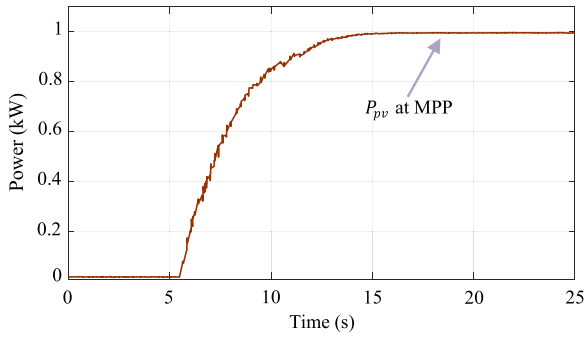

Fig. 17. Experimental responses of PV power from the right side of MPP, using the proposed controller based on (33).

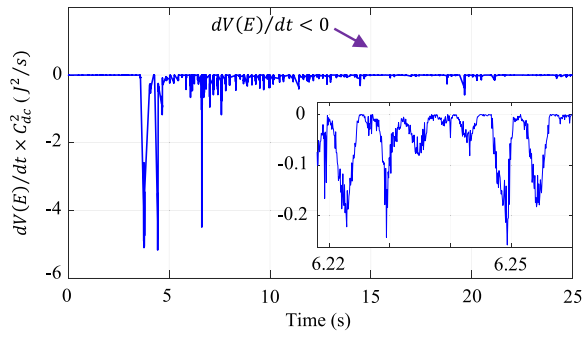

Fig. 18. Experimental result of derivative of Lyapunov function from the right side of MPP, using the proposed controller based on (33). In order to help visualising the full range on the graph, it has been multiplied by C_{dc}^2.

power flow is interrupted. Once the adaptive controller and the P&O MPPT algorithm are enabled, Figs. 19 and 20 show the PV voltage tracking response and the PV power starting from the left side. Moreover, Fig. 21 shows the derivative of Lyapunov function where it can be seen that it remains negative, meaning an achievement of the global stability.

In addition, Fig. 22 shows the comparison of both dc-link voltage controllers; PI controller and the adaptive controller, where it can be observed that both reach the MPP simultaneously. It should be noted that the parameters used for the PI controller ($K_p = 8 \times 10^{-5}$ and $K_I = 8,5 \times 10^{-4}$) are adjusted carefully in STC with respect to different constraints of dynamic performances, among them to avoid the overshoot of step responses of the dc-link voltage. Whereas the adaptive

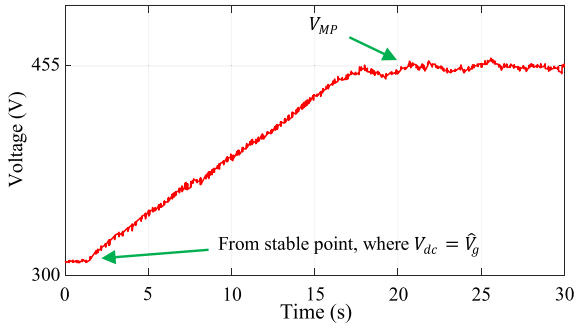

Fig. 19. Experimental responses of PV voltage from the left side of MPP, using the proposed controller based on (33).

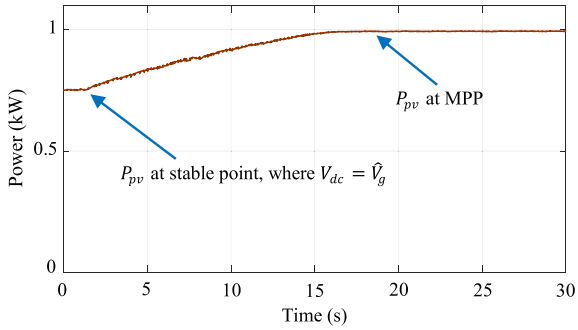

Fig. 20. Experimental responses of PV power from the left side of MPP, using the proposed controller based on (33).

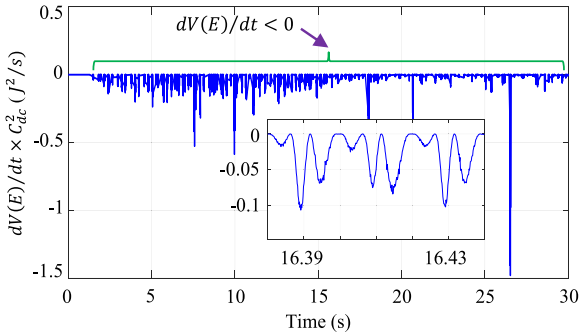

Fig. 21. Experimental result of derivative of Lyapunov function from the left side of MPP, using the proposed controller based on (33). In order to help visualising the full range on the graph, it has been multiplied by C_{dc}^2.

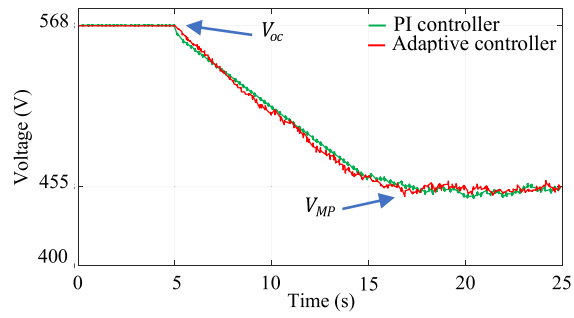

Fig. 22. Experimental start waveforms comparison of dc-link voltage for both controllers (PI controller and adaptive controller).

dc-link voltage controller proposed in this article (as an application of the analityc stability study) depends on the P-V curve characteristic of the PV string. The current control loop bandwidth is around 500 Hz and for the dc-link voltage control loop is imposed by the MPPT frequency, which is selected as: $f_{MPPT} =$ 10 Hz. Consequently, the interaction between the internal current control loop and the external dc-link voltage control loop is not considered.

V. Conclusion

In this article, a stability analysis for single-stage single-phase grid-connected PV inverters has been presented. It was demonstrated analytically that the nonlinearity of the PV string's P-V curve is significantly affecting the system stability. The study is based on the Lyapunov function, which was formed from the variation of stored energy in the dc-link capacitor. Hence, the derivative represents the variation of the PV power in terms of the dc-link capacitor voltage difference. Typically, without using a voltage controller, the right side of MPP on the P-V curve ($V_{pv} > V_{MP}$) is stable, while the left side of MPP ($V_{pv} < V_{MP}$) remains unstable. Consequently, adding a PI controller to regulate directly the energy across the dc-link capacitor makes the system globally stable, regardless of the location of the operating point. Hence, the stability analysis presented in this article proved that the reverse error signal at the input of the dc-link voltage controller derives from the stability issue.

A simulation test was carried out to validate the analytical demonstration. Furthermore, an adaptive dc-link voltage controller based on the P-V curve of the PV string has been proposed as an application in this article. The experimental validations confirm the feasibility of the study, once a new nonlinear controller is designed for the dc-link voltage.

References

[1] R. K. Jones and S. Kurtz, "Optimizing the configuration of photovoltaic plants to minimize the need for storage," *IEEE J. Photovolt.*, vol. 12, no. 3, pp. 860–870, May 2022.

[2] L. Callegaro, G. Konstantinou, C. A. Rojas, N. F. Avila, and J. E. Fletcher, "Testing evidence and analysis of rooftop PV inverters response to grid disturbances," *IEEE J. Photovolt.*, vol. 10, no. 6, pp. 1882–1891, Nov. 2020.

[3] A. Ahmad, H. D. Tafti, G. Konstantinou, B. Hredzak, and J. E. Fletcher, "Distributed photovoltaic inverters' response to voltage phase-angle jump," *IEEE J. Photovolt.*, vol. 12, no. 1, pp. 429–436, Jan. 2022.

[4] O. Ceylan, S. Paudyal, and I. Pisica, "Nodal sensitivity-based smart inverter control for voltage regulation in distribution feeder," *IEEE J. Photovolt.*, vol. 11, no. 4, pp. 1105–1113, Jul. 2021.

[5] G. E. Valderrama et al., "A single-phase asymmetrical T-type five-level transformerless PV inverter," *IEEE J. Emerg. Sel. Topics Power Electron.*, vol. 6, no. 1, pp. 140–150, Mar. 2018, doi: 10.1109/JESTPE.2017.2726989.

[6] A. Sarikhani, M. M. Takantape, and M. Hamzeh, "A transformerless common-ground three-switch single-phase inverter for photovoltaic systems," *IEEE Trans. Power Electron.*, vol. 35, no. 9, pp. 8902–8909, Sep. 2020.

[7] M. N. H. Khan et al., "Transformerless inverter topologies for single-phase photovoltaic systems: A comparative review," *IEEE J. Emerg. Sel. Topics Power Electron.*, vol. 8, no. 1, pp. 805–835, Mar. 2020.

[8] M. Kamalirad, H. Iman-Eini, B. Farhangi, and S. Bacha, "A reliable three-phase transformerless grid-connected PV inverter with inductive DC link," *IEEE J. Photovolt.*, vol. 8, no. 5, pp. 1305–1312, Sep. 2018.

[9] B. Karanayil, S. Ceballos, and J. Pou, "Maximum power point controller for large-scale photovoltaic power plants using central inverters under partial shading conditions," *IEEE Trans. Power Electron.*, vol. 34, no. 4, pp. 3098–3109, Apr. 2019.

[10] C. F. Abe, J. B. Dias, G. Notton, and P. Poggi, "Computing solar irradiance and average temperature of photovoltaic modules from the maximum power point coordinates," *IEEE J. Photovolt.*, vol. 10, no. 2, pp. 655–663, Mar. 2020.

[11] M. Castilla, J. Miret, J. Matas, L. G. de Vicuña, and J. M. Guerrero, "Linear current control scheme with series resonant harmonic compensator for single-phase grid-connected photovoltaic inverters," *IEEE Trans. Ind. Electron.*, vol. 55, no. 7, pp. 2724–2733, Jul. 2008.

[12] T. Hornik and Q.-C. Zhong, "A current-control strategy for voltage-source inverters in microgrids based on H∞ and repetitive control," *IEEE Trans. Power Electron.*, vol. 26, no. 3, pp. 943–952, Mar. 2011.

[13] S.-Y. Park, C.-L. Chen, J.-S. Lai, and S.-R. Moon, "Admittance compensation in current loop control for a grid-tie LCL fuel cell inverter," *IEEE Trans. Power Electron.*, vol. 23, no. 4, pp. 1716–1723, Jul. 2008.

[14] S. Golestan, J. Guerrero, and J. Vasquez, "Single-phase PLLs: A review of recent advances," *IEEE Trans. Power Electron.*, vol. 32, no. 12, pp. 9013–9030, Dec. 2017.

[15] M. Rajeev and V. Agarwal, "Analysis and control of a novel transformerless microinverter for PV-grid interface," *IEEE J. Photovolt.*, vol. 8, no. 4, pp. 1110–1118, Jul. 2018.

[16] M. Merai, M. W. Naouar, and I. Slama-Belkhodja, "An improved DC-link voltage control strategy for grid connected converters," *IEEE Trans. Power Electron.*, vol. 33, no. 4, pp. 3575–3582, Apr. 2018.

[17] C. Wang, X. Li, L. Guo, and Y. W. Li, "A nonlinear-disturbance-observer-based DC-bus voltage control for a hybrid AC/DC microgrid," *IEEE Trans. Power Electron.*, vol. 29, no. 11, pp. 6162–6177, Nov. 2014.

[18] Y. Gui et al., "Improved DC-link voltage regulation strategy for grid-connected converters," *IEEE Trans. Ind. Electron.*, vol. 68, no. 6, pp. 4977–4987, Jun. 2021.

[19] M. Karimi-Ghartemani, S. A. Khajehoddin, P. Jain, and A. Bakhshai, "A systematic approach to DC-bus control design in single-phase grid-connected renewable converters," *IEEE Trans. Power Electron.*, vol. 28, no. 7, pp. 3158–3166, Jul. 2013.

[20] S. Eren, M. Pahlevani, A. Bakhshai, and P. Jain, "An adaptive droop DC-bus voltage controller for a grid-connected voltage source inverter with LCL filter," *IEEE Trans. Power Electron.*, vol. 30, no. 2, pp. 547–560, Feb. 2015.

[21] S. A. Khajehoddin, M. Karimi-Ghartemani, P. K. Jain, and A. Bakhshai, "DC-bus design and control for a single-phase grid-connected renewable converter with a small energy storage component," *IEEE Trans. Power Electron.*, vol. 28, no. 7, pp. 3245–3254, Jul. 2013.

[22] T.-F. Wu, C.-H. Chang, L.-C. Lin, G.-R. Yu, and Y.-R. Chang, "DC-bus voltage control with a three-phase bidirectional inverter for DC distribution systems," *IEEE Trans. Power Electron.*, vol. 28, no. 4, pp. 1890–1899, Apr. 2013.

[23] C. Meza, D. Biel, D. Jeltsema, and J. M. A. Scherpen, "Lyapunov-based control scheme for single-phase grid-connected PV central inverters," *IEEE Trans. Control Syst. Technol.*, vol. 20, no. 2, pp. 520–529, Mar. 2012, doi: 10.1109/TCST.2011.2114348.

[24] M. Rezkallah, S. K. Sharma, A. Chandra, B. Singh, and D. R. Rousse, "Lyapunov function and sliding mode control approach for the solar-PV grid interface system," *IEEE Trans. Ind. Electron.*, vol. 64, no. 1, pp. 785–795, Jan. 2017.

[25] K. Ma, W. Chen, M. Liserre, and F. Blaabjerg, "Power controllability of a three-phase converter with an unbalanced AC source," *IEEE Trans. Power Electron.*, vol. 30, no. 3, pp. 1591–1604, Mar. 2015.

[26] J. Chavarria, D. Biel, F. Guinjoan, C. Meza, and J. J. Negroni, "Energy-balance control of PV cascaded multilevel grid-connected inverters under level-shifted and phase-shifted PWMs," *IEEE Trans. Ind. Electron.*, vol. 60, no. 1, pp. 98–111, Jan. 2013.

[27] M. Reveles-Miranda, M. Flota-Bañuelos, F. Chan-Puc, V. Ramirez-Rivera, and D. Pacheco-Catalán, "A hybrid control technique for harmonic elimination, power factor correction, and night operation of a grid-connected PV inverter," *IEEE J. Photovolt.*, vol. 10, no. 2, pp. 664–675, Mar. 2020.

[28] N. A. Ashtiani, S. M. Azizi, and S. A. Khajehoddin, "Robust control design for high-power density PV converters in weak grids," *IEEE Trans. Control Syst. Technol.*, vol. 27, no. 6, pp. 2361–2373, Nov. 2019, doi: 10.1109/TCST.2018.2867212.

[29] R. Errouissi, A. Al-Durra, and S. M. Muyeen, "Design and implementation of a nonlinear PI predictive controller for a grid-tied photovoltaic inverter," *IEEE Trans. Ind. Electron.*, vol. 64, no. 2, pp. 1241–1250, Feb. 2017.

[30] N. E. Zakzouk, A. K. Abdelsalam, A. A. Helal, and B. W. Williams, "PV single-phase grid-connected converter: DC-link voltage sensorless prospective," *IEEE J. Emerg. Sel. Topics Power Electron.*, vol. 5, no. 1, pp. 526–546, Mar. 2017.

[31] Y. Sun, Y. Liu, M. Su, W. Xiong, and J. Yang, "Review of active power decoupling topologies in single-phase systems," *IEEE Trans. Power Electron.*, vol. 31, no. 7, pp. 4778–4794, Jul. 2016, doi: 10.1109/TPEL.2015.2477882.

[32] I. Serban, "Power decoupling method for single-phase H-bridge inverters with no additional power electronics," *IEEE Trans. Ind. Electron.*, vol. 62, no. 8, pp. 4805–4813, Aug. 2015, doi: 10.1109/TIE.2015.2399274.

[33] F. el Aamri et al., "A direct maximum power point tracking method for single-phase grid connected PV inverters," *IEEE Trans. Power Electron.*, vol. 33, no. 10, pp. 8961–8971, Oct. 2018, doi: 10.1109/TPEL.2017.2780858.

[34] E. Rodriguez-Diaz, F. D. Freijedo, J. C. Vasquez, and J. M. Guerrero, "Analysis and comparison of notch filter and capacitor voltage feedforward active damping techniques for LCL grid-connected converters," *IEEE Trans. Power Electron.*, vol. 34, no. 4, pp. 3958–3972, Apr. 2019.

[35] H. Komurcugil, N. Altin, S. Ozdemir, and I. Sefa, "An extended lyapunov-function-based control strategy for single-phase UPS inverters," *IEEE Trans. Power Electron.*, vol. 30, no. 7, pp. 3976–3983, Jul. 2015, doi: 10.1109/TPEL.2014.2347396.

[36] M. Ciobotaru, R. Teodorescu, and F. Blaabjerg, "Control of single-stage single-phase PV inverter," *EPE J.*, vol. 16, no. 3, pp. 20–26, Sep. 2006, doi: 10.1080/09398368.2006.11463624.

[37] H. Schmidt, B. Burger, U. Bussemas, and S. Elies, "How fast does an MPP tracker really need to be?," in *Proc. 24th EuPVSEC*, 2009, pp. 3273–3276.